chemosensors

Article

$BiVO_4$-Based Photoelectrochemical Sensors for the Detection of Diclofenac: The Role of Doping, Electrolytes and Applied Potentials

Milda Petruleviciene [1,*], Irena Savickaja [1], Jelena Kovger-Jarosevic [1], Monika Skruodiene [1], Jurga Juodkazyte [1], Simonas Ramanavicius [1] and Arunas Ramanavicius [1,2,*]

[1] Centre for Physical Sciences and Technology, Sauletekio av. 3, LT-10257 Vilnius, Lithuania; irena.savickaja@ftmc.lt (I.S.); jelena.kovger@ftmc.lt (J.K.-J.); monika.skruodiene@ftmc.lt (M.S.); jurga.juodkazyte@ftmc.lt (J.J.); simonas.ramanavicius@ftmc.lt (S.R.)
[2] Institute of Chemistry, Faculty of Chemistry and Geosciences, Vilnius University, LT-01513 Vilnius, Lithuania
* Correspondence: milda.petruleviciene@ftmc.lt (M.P.); arunas.ramanavicius@chf.vu.lt (A.R.)

Abstract: This study presents the findings of an investigation into the characteristics and capabilities of $BiVO_4$ and Mo-doped $BiVO_4$ coatings for the detection of diclofenac (DCF). In this study, a neutral sodium sulfate electrolyte and an alkaline sodium borate buffer were selected, and a range of potentials were employed to ascertain the impact of diverse conditions on the sensing performance of diclofenac. The introduction of Mo-doping had a profound impact on the photoelectrochemical response of the $BiVO_4$ coating. However, it was observed that Mo-doping resulted in an increase in the adsorption of diclofenac oxidation products on the surface of the photoanode, which in turn led to a negative blocking effect. To evaluate the structural and morphological properties of the coatings, X-ray diffraction analysis (XRD), scanning electron microscopy (SEM), and energy dispersive analysis (EDX) were conducted. The photoelectrochemical properties were evaluated through the use of cyclic voltammetry (CV), electrochemical impedance spectroscopy (EIS) and chronoamperometry (CA). An increase in the photocurrent density of $BiVO_4$ was observed in response to an increase in the concentration of diclofenac within a range of 0.1 to 1 mg L^{-1} during the sensing experiments. However, at higher concentrations, saturation of diclofenac was observed at the photoelectrode/electrolyte interface. The results of selectivity experiments demonstrated that the nature of the electrolyte has a significant impact on the selectivity of designed photoelectrochemical sensors.

Keywords: photoelectrochemical sensing; $BiVO_4$; detection; sensitivity; oxidation; diclofenac

Citation: Petruleviciene, M.; Savickaja, I.; Kovger-Jarosevic, J.; Skruodiene, M.; Juodkazyte, J.; Ramanavicius, S.; Ramanavicius, A. $BiVO_4$-Based Photoelectrochemical Sensors for the Detection of Diclofenac: The Role of Doping, Electrolytes and Applied Potentials. *Chemosensors* **2024**, *12*, 249. https://doi.org/10.3390/chemosensors12120249

Received: 1 October 2024
Revised: 18 November 2024
Accepted: 25 November 2024
Published: 27 November 2024

1. Introduction

Pharmaceutical pollutants, including antibiotics, analgesics, anti-inflammatory drugs, and hormone-related compounds have become emerging contaminants in water sources due to their widespread use in healthcare and agriculture [1,2]. These compounds enter the environment through wastewater discharge, improper disposal of unused medications, and agricultural and industry runoff [3,4]. Pharmaceutical pollutants in the environment have a hazardous effect on both human health and ecosystems [5]. Once present in aquatic ecosystems, pharmaceuticals are often resistant to conventional water treatment processes, leading to their persistent accumulation in water bodies [6–8]. For humans, chronic exposure to trace levels of pharmaceuticals through drinking water or contaminated food sources raises concerns about potential long-term health effects, such as antibiotic resistance and hormonal imbalances [9–11].

Given the increasing prevalence of pharmaceutical contaminants and their potential impacts, there is a critical need for sensitive, selective, and reliable methods to detect and monitor these compounds in complex matrices, such as wastewater and biological fluids. Conventional analytical techniques, such as high-performance liquid chromatography

(HPLC), liquid chromatography coupled with tandem mass spectrometry (LC-MS/MS), and UV-visible spectroscopy, are associated with significant time consumption, high operational costs, and the necessity for skilled personnel. Furthermore, their application in field operations is limited due to their complexity. In contrast, electrochemical sensors have attracted considerable attention owing to their rapid response, high sensitivity and selectivity, and promising potential for real-time, on-site detection [12,13].

Photoelectrochemical (PEC) sensors, with their ability to achieve low detection limits and adaptability for in situ monitoring, offer a promising solution for addressing this environmental and public health challenge [14]. The development of advanced PEC sensors for pharmaceutical detection holds significant importance for safeguarding water quality and protecting both human and environmental health. Photoelectrochemical (PEC) sensors are based on a reaction on the surface of an electrode under light illumination, leading to appearance of a signal—a photocurrent [15]. However, to achieve high selectivity and stability in complex environments remains a key challenge. Photoelectrochemical (PEC) systems have been used to detect a variety of pharmaceutical compounds, including antibiotics (e.g., tetracycline, ciprofloxacin), analgesics (e.g., acetaminophen), anti-inflammatory drugs (e.g., ibuprofen), and hormone-related compounds (e.g., estradiol) [16–22].

The sensitivity and selectivity of the sensor depends on the nature of the photoanodes. A variety of photoanodes can be employed, including titanium dioxide (TiO_2), zinc oxide (ZnO), bismuth vanadate ($BiVO_4$), and tungsten oxide (WO_3) [23–28]. These are commonly employed in PEC sensors for pharmaceutical detection, and frequently enhanced through doping, composites (e.g., with graphene), or co-catalysts, which improve sensitivity, selectivity, and stability [29]. The choice of semiconductor is dependent on the pharmaceutical compound under investigation, the desired wavelength range (ultraviolet or visible), and the prevailing environmental conditions. Moreover, the sensitivity and selectivity of the photoanodes are affected by the applied potential within the PEC system and the nature of the electrolytes [18]. The nature of the electrolytes and their pH are of great importance, as certain ions may be oxidized on the surface of the photoanode, resulting in the production of radicals that can participate in oxidation reactions with organic compounds [30]. The behavior of different types of pharmaceutical compounds in electrolytes of various pH can vary considerably, because they may form stable complexes [31,32].

$BiVO_4$ is a photoelectrochemically active material with a bandgap of approximately 2.4–2.5 eV, which enables it to absorb a broad spectrum of visible light [33]. The valence band (VB) of $BiVO_4$ is positioned at approximately 2.6 V, which provides photogenerated holes with sufficient energy to drive a variety of oxidation reactions [34]. However, $BiVO_4$ has certain limitations, primarily due to the rapid recombination of charge carriers, which results in a reduction in signal intensity [35]. In order to enhance the PEC performance of $BiVO_4$, doping with elements such as W and Mo is employed. These dopants reduce charge carrier recombination by increasing the availability of free electrons, thereby improving the n-type semiconductor properties of $BiVO_4$ [36].

In this study, a PEC sensor was formed using $BiVO_4$ and Mo-doped $BiVO_4$ coatings on an FTO conductive substrate. The sensing performance of the photoanodes was investigated for the detection of diclofenac in sodium sulfate (pH = 7) and sodium borate buffer (pH = 9). This study presents novel findings and an analysis of the influence of the doping of $BiVO_4$, the nature of the electrolyte, and the applied potentials of the sensing performance. The coatings were characterized using XRD, SEM, and EDX analysis. The photoelectrochemical properties were evaluated using cyclic voltammetry (CV), electrochemical impedance spectroscopy (EIS), and chronoamperometry (CA) techniques. The sensing performance was analyzed using chronoamperometry techniques under chopped light illumination with electrolytes containing different amounts of diclofenac. It is expected that the presented findings will prove valuable in the development of PEC sensors for the detection of pharmaceutical compounds.

2. Experimental Section

2.1. Materials

Bismuth (III) nitrate pentahydrate ($Bi(NO_3)_3 \times 5\ H_2O$) (Carl Roth, Karlsruhe, Germany), ammonium vanadate (NH_4VO_3) (Acros Organics, Kandel, Germany), nitric acid (H_3NO_3) (Reachmen, Bratislava, Slovakia), ammonium molybdate heptahydrate ($(NH_4)_6Mo_7O_{24} \times 7\ H_2O$) (Chempur, Piekary Slaskie, Poland), citric acid ($C_6H_8O_6$) (Chempur, Piekary Slaskie, Poland), polyvinyl alcohol (PVA) (Chempur, Piekary Slaskie, Poland), acetic acid (CH_3COOH) (Chempur, Piekary Slaskie, Poland), sodium sulfate (Na_2SO_4) (Acros Organics, Kandel, Germany), sodium borate decahydrate ($Na_2B_4O_7 \times 10\ H_2O$) (Tarchem, Tornowskie Gory, Poland), boric acid (H_3BO_3) (Chempur, Piekary Slaskie, Poland), sodium diclofenac ($C_{14}H_{10}Cl_2NNaO_2$) (Farmalabor, Assago, Italy), Ibuprofen ($C_{13}H_{18}O_2$) (Farmalabor, Assago, Italy), and dopamine ($C_8H_{11}NO_2$) (Fluorochem, Assago, UK) were used as received from suppliers without further purification.

2.2. Synthesis of $BiVO_4$ and Mo_$BiVO_4$ Coatings

Bismuth vanadate ($BiVO_4$) coatings were deposited onto a conducting glass substrate (fluorine-doped tin oxide, FTO) using a sol-gel method combined with dip-coating (Figure 1). The solution was prepared from bismuth (III) nitrate ($Bi(NO_3)_3 \times 5\ H_2O$), ammonium vanadate ($NH_4VO_3$), nitric acid ($HNO_3$, 67%), ammonium molybdate ($(NH_4)_6Mo_7O_{24} \times 4\ H_2O$), citric acid ($C_6H_8O_6$), acetic acid ($CH_3COOH$, 99.9%), and polyvinyl alcohol (PVA). All chemicals were used as received without further purification. Initially, 2.94 g of $Bi(NO_3)_3 \times 5\ H_2O$ and 0.702 g of NH_4VO_3 (in a 1:1 molar ratio) were dissolved in 23% HNO_3. Then, 2.52 g of citric acid was added under constant stirring, resulting in a clear blue solution. To achieve the desired sol-gel viscosity, 1 g of PVA and 3 mL of acetic acid were introduced, and the mixture was stirred with a magnetic stirrer for 24 h at 50 °C. For molybdenum-doped $BiVO_4$ coatings (Mo_$BiVO_4$), 0.7489 g of ammonium molybdate, corresponding to 10 atomic % Mo, was added to the solution after 4 h of stirring. Then the formed sol was stirred for another 24 h at room temperature.

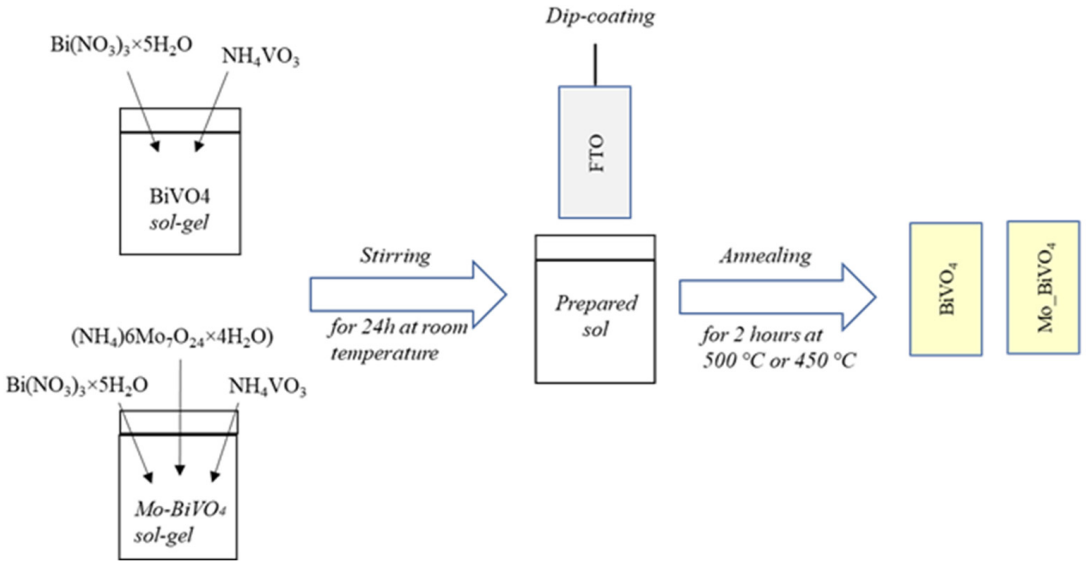

Figure 1. Synthesis scheme for preparation of $BiVO_4$ and Mo_$BiVO_4$ coatings.

The resulting sol was used to deposit thin films on the FTO substrate. Before coating, the FTO glass was thoroughly cleaned in acetone, isopropanol, and water using an ultrasonic bath for 15 min in each solvent. The dip-coating process was performed using a Nadetech ND-DC 11/1 dip-coater, immersing the FTO at a rate of 100 mm/min into the $BiVO_4$ or Mo-doped $BiVO_4$ sol. The immersed substrate was kept in the sol for 1 min before being withdrawn at the same rate. The $BiVO_4$ and Mo-doped $BiVO_4$ coatings were

annealed in ambient air for 2 h at 500 °C and 450 °C, respectively. To increase the coating thickness, the process was repeated twice.

2.3. Structural and Morphological Analysis

The composition and structure of the synthesized coatings were examined using a SmartLab X-ray diffractometer (Rigaku, Neu-Isenburg, Germany) with a 9 kW rotating copper anode X-ray tube. The analysis was conducted over a 2θ range of 20–80°, utilizing the grazing incidence X-ray diffraction (XRD) method, with a fixed angle (ω) of 0.5° between the parallel X-ray beam and the sample surface. Phase identification was performed using Match software (3.10.2.173), referencing the Crystallography Open Database (COD).

The morphology of the coatings was characterized using a Helios NanoLab dual beam workstation, equipped with an EDX spectrometer (Oxford Instruments, Amsterdam, The Netherlands). Mapping and elemental analysis were carried out at 10 kV and 20 kV, respectively.

2.4. Photoelectrochemical Investigations

Cyclic voltammetry, electrochemical impedance spectroscopy, and chronoamperometry measurements were conducted using a potentiostat/galvanostat Zennium/Zahner Xpot (Zahner Elektrik, Kronach, Germany) and a three-electrode electrochemical cell. The experiments were conducted in electrolytes comprising 0.1 M Na_2SO_4 (SS) and 0.2 M sodium borate buffer (SBB). $BiVO_4$ and Mo_$BiVO_4$ films deposited on FTO substrates were used as working electrodes. A silver/silver chloride electrode with a 3 M KCl solution (Ag/AgCl) and a platinum plate (1 × 1 cm^2) were employed as the reference and counter electrodes, respectively. All potential values stated in this paper are reported versus Ag/AgCl, unless otherwise indicated. The surface (1 cm^2) of the working electrode was illuminated with an LED solar simulator (Redox.me), with a light intensity of 100 mW cm^{-2}. The Nyquist plots were measured at 0.7 V and 0.6 V in SS and SBB, respectively, with an AC amplitude of 10 mV, and within a frequency range from 10^4 to 0.1 Hz under illumination.

Photoelectrochemical detection experiments were conducted in 0.1 M Na_2SO_4 and 0.2 M sodium borate buffer electrolytes containing 0.1, 0.5, 1, 5, and 10 mg L^{-1} of diclofenac using chronoamperometry under chopped light illumination experiments with 30 s dark/light intervals using $BiVO_4$ and Mo_$BiVO_4$ photoanodes. In order to evaluate the impact of applied potentials on PEC sensing performance, a series of experiments were conducted, applying potentials of 1.4, 1, and 0.6 V for samples analyzed in the 0.1 M Na_2SO_4 electrolyte. In the case of the 0.2 M sodium borate buffer, the applied potentials were 1, 0.6, and 0.2 V.

Selectivity experiments were performed with $BiVO_4$ using the chronoamperometric technique at 1.4 and 1 V in SS and at 1 and 0.6 V in SBB. In selectivity tests 100 µL of 50 mgL^{-1} diclofenac, 50 mg L^{-1} dopamine, 50 mg L^{-1} diclofenac, 50 mg L^{-1} dopamine, 5 mg L^{-1} ibuprofen, 50 mg L^{-1} diclofenac, and finally 1 mL of 5 mg L^{-1} ibuprofen were sequentially added every 60 s to SS and SBB electrolytes.

3. Results and Discussion

3.1. Structural and Morphological Properties of $BiVO_4$ and Mo_$BiVO_4$ Coatings

The crystalline structure and morphology of the synthesized coatings were evaluated through the application of X-ray diffraction analysis and scanning electron microscopy (Figure 2a–c). Figure 2a,b present scanning electron microscopy images of $BiVO_4$ and Mo-doped $BiVO_4$ coatings, respectively. The Mo_$BiVO_4$ coating consists of elongated particles with a diameter of approximately 200–800 nm. In contrast, the pure $BiVO_4$ coating is composed of smaller particles that are interconnected. The XRD analysis confirmed that both coatings have a monoclinic crystalline structure, in accordance with the Crystallography Open Database (COD) No. 9013436 (Figure 2c). Peaks corresponding to $BiVO_4$ are marked by asterisks (*). Additionally, peaks (marked as—♦) corresponding to SnO_2 (COD: 9009082)

are observed. To confirm the Mo-doping effect, an EDX analysis was carried out, and the EDX mapping results demonstrated that the doping with Mo was successful (Figure 2d,e).

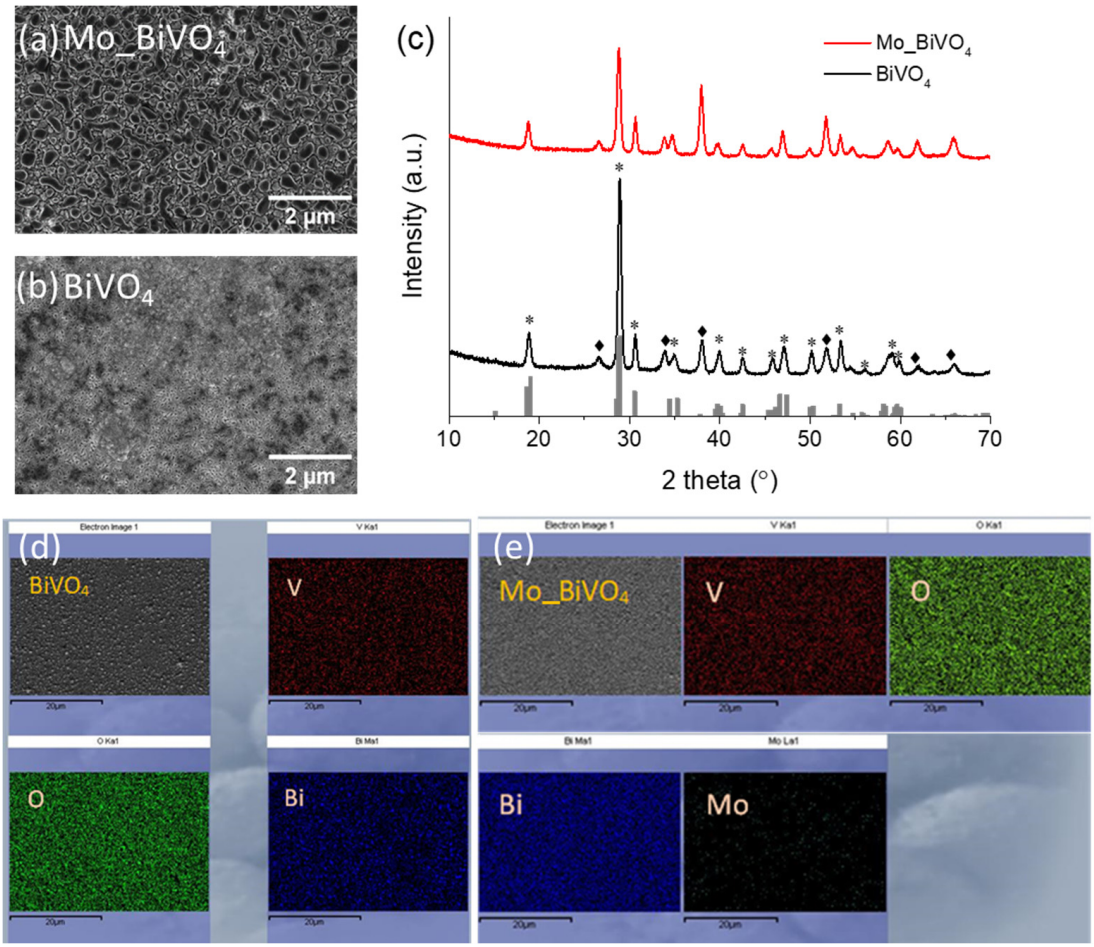

Figure 2. (**a**,**b**) SEM images, (**c**) XRD and (**d**,**e**) EDX results of $BiVO_4$ and Mo_$BiVO_4$ coatings.

3.2. Photoelectrochemical Investigations of $BiVO_4$ and Mo_$BiVO_4$ Coatings

The photoresponse of the synthesized coatings was evaluated using cyclic voltammetry. The cyclic voltammograms of the $BiVO_4$ and Mo_$BiVO_4$ coatings recorded in 0.1 M Na_2SO_4 and 0.2 M sodium borate buffer are presented in Figures 3a and 3b, respectively. In the absence of light, both coatings exhibited minimal current. In the presence of light, the Mo-doped coatings in the SS electrolyte exhibited a photocurrent of approximately 0.52 mA cm^{-2} at 1.4 V, while the pure $BiVO_4$ reached a value of approximately 0.5 mA cm^{-2}. Another distinction can be seen in the shapes of the curves, where the photocurrent of Mo_$BiVO_4$ started to increase at a lower applied potential of about 0.1 V, whereas for $BiVO_4$ the increase started at 0.4 V. The curve of Mo_$BiVO_4$ is markedly steeper, indicating a considerably faster charge transfer (Figure 3a). Similar regularities were observed in the 0.2 M SBB electrolyte, where a faster increase in photocurrent was also found for the Mo-doped coating. The photocurrent in the SBB is slightly lower due to the differing nature and pH of the electrolytes (Figure 3b). In the borate buffer at pH 9, the primary oxidation reaction is likely to be water oxidation [37,38]; however, in sodium sulfate (pH 7), sulfate ions may be oxidized with greater ease on the surface of the photoanode, as sulfate oxidation is typically more favorable than water oxidation, leading to an elevated photocurrent [39–42].

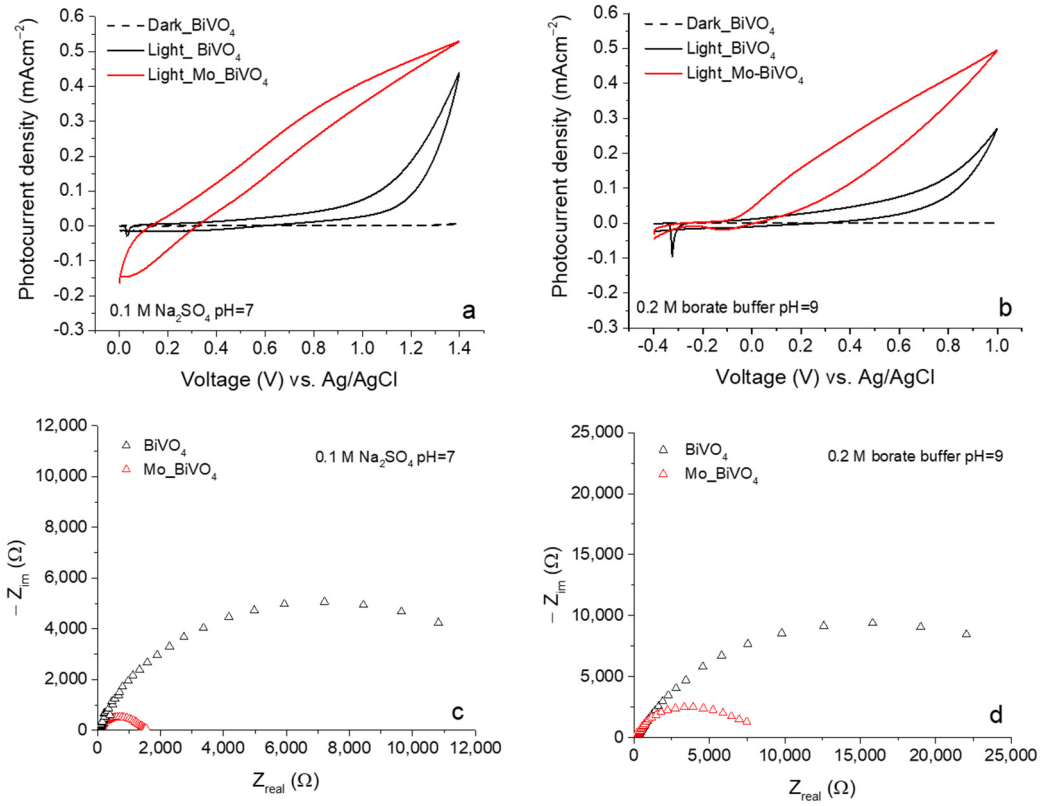

Figure 3. Cyclic voltammograms and electrochemical impedance spectroscopy results of $BiVO_4$ and Mo_$BiVO_4$ coatings in 0.1 M Na_2SO_4 (**a**,**c**) and 0.2 M sodium borate buffer (**b**,**d**). Scan rate of CV 50 mVs^{-1}.

Electrochemical impedance spectroscopy (EIS) experiments were conducted to quantify the charge transfer resistance of the two coatings in the 0.1 M SS and 0.2 M SBB electrolytes. The charge transfer resistance (R_{ct}) was observed to be lower in the sodium sulfate electrolyte, reaching 1700 Ω and 12,000 Ω for the Mo_$BiVO_4$ and $BiVO_4$ coatings, respectively (Figure 3c,d). However, in the SBB, the R_{ct} is more than two times higher for both samples, indicating a slowed charge transfer kinetic in the alkaline electrolyte. The doping of $BiVO_4$ with Mo is typically employed to enhance the transport of charges within the bulk, thereby increasing the electrical conductivity. The replacement of V^{5+} with Mo^{6+} results in the formation of donor states, which in turn leads to an improvement in electron mobility. This enhanced conductivity is reflected in the EIS measurements, wherein the Mo-doped $BiVO_4$ exhibits a lower R_{ct} compared to the undoped $BiVO_4$, indicating superior charge transfer.

The results of the chronoamperometry under chopped light illumination demonstrated a similar tendency to those observed in previous experiments. The transient photocurrent was found to be almost two times higher for Mo-doped coatings (Figure 4a,b). In the SBB, the photocurrent decreased more rapidly under light illumination for both coatings, indicating that the recombination of charge carriers occurred more quickly in the case of an alkaline electrolyte. $BiVO_4$ is sensitive to pH changes, and its surface properties (e.g., surface states, band edge positions, and recombination rates) can vary depending on the electrolyte [43]. Therefore, the higher R_{ct} in the SBB is predominantly due to the different oxidation reactions and band shifts.

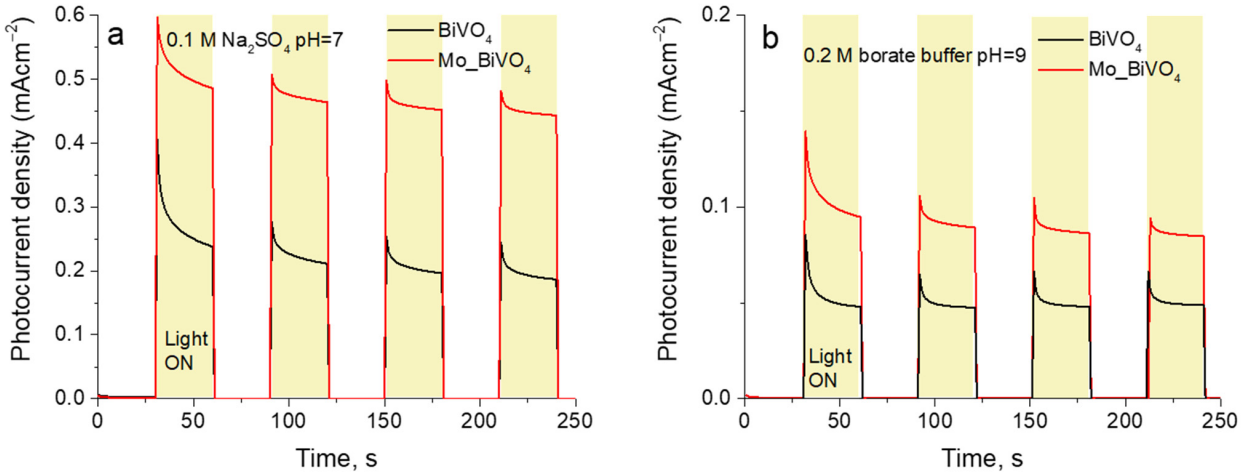

Figure 4. Chronoamperometry under chopped light illumination results in 0.1 M Na_2SO_4 (**a**) and 0.2 M sodium borate buffer (**b**) at 1.4 V and 1 V vs. Ag/AgCl, respectively.

3.3. Photoelectrochemical Sensing of Diclofenac

The PEC detection of diclofenac with $BiVO_4$ and Mo_$BiVO_4$ was studied using chronoamperometry under chopped illumination in sodium sulfate and sodium borate buffer containing 0.1, 0.5, 1, 5, and 10 mg L^{-1} of DCF. The experiments were conducted with the application of varying potentials in order to find the optimal conditions and the impact of such conditions on the sensing performance. Figure 5a–d present the photocurrent versus the concentration of diclofenac. The values of the photocurrent were obtained from the midpoint of the second step of transient photocurrents, as presented in the (Supplementary Figures S1 and S2). As illustrated in Figure 5a,b, the photocurrent of $BiVO_4$ increases with increasing concentration of DCF for all applied potentials, namely 1.4, 1, and 0.6 V in sodium sulfate and 1, 0.6, and 0.2 V in sodium borate buffer. At low concentrations of DCF, rapid oxidation occurred on the $BiVO_4$ surface, resulting in an increase in photocurrent density. Upon reaching a concentration of 1 mg L^{-1}, the photocurrent density exhibited a gradual increase, approaching a maximum value. It can be postulated that at elevated concentrations of DCF, a point is reached where the oxidation reaction is no longer feasible within the allotted time. Consequently, the interfacial charge transfer resistance increases, resulting in a saturation of the photocurrent density. A comparative analysis of the SS and SBB electrolytes reveals that at higher potential (1 V) in SBB, the photocurrent density increases more steeply with increasing concentrations of diclofenac within the range of 0 to 1 mg L^{-1}.

The results of the Mo_$BiVO_4$ coatings, as presented in Figure 5c,d, are strikingly different. Upon application of 1.4 V in sodium sulfate, a dramatic decrease of the photocurrent is observed in the electrolyte containing 0.1 mg L^{-1} of DCF and a further slow decrease is observed with increase in diclofenac concentration in the SS electrolyte (Figure 5c). In the case of SBB, however, a sudden increase in photocurrent was observed at 1 V upon addition of DCF (Figure 5d). With further increase in DCF concentration, the photocurrent decreased until it reached a saturation level comparable to that of $BiVO_4$. This phenomenon can be explained by the blocking off of the Mo_$BiVO_4$ surface, which may have been caused by the adsorption of DCF or DCF oxidation products on the electrode. The findings of reference [44] support this assumption, indicating that an increase in the concentration of the organic compound results in enhanced resistance and a reduction in photocurrent. This layer can hinder light absorption and limit the interaction between the photoanode surface and the electrolyte, reducing the available active sites for the photoelectrochemical reaction and thus decreasing the photocurrent. The SEM images (Figure 2a,b) clearly demonstrate that the morphology of the $BiVO_4$ and Mo_$BiVO_4$ coatings is markedly different, suggesting that the adsorption of organic compounds on their surfaces may also be different. With regard to the lower potentials, it can be observed that in SBB, the tendencies are

the same. However, in SS, the results are random, with no discernible tendencies. As previously demonstrated in our research, the dominant reaction occurring on the surface of the $BiVO_4$ photoanode in the presence of the sodium sulfate electrolyte is sulfate oxidation to persulfate ($SO_4^{2-} \rightarrow S_2O_8^{2-}$) [39–42], with the competing water oxidation reaction. The random distribution of photocurrent values in the case of Mo_$BiVO_4$ (Figure 5c) may be attributed to the aforementioned sulfate oxidation reaction, which is slowed down by the presence of DCF on the photoanode surface. The different morphology of the coatings, in addition to the doping of Mo, can give rise to disparate surface states, which affect the interactions with DCF. This phenomenon gives rise to the observed random distribution of the photocurrent values vs. DCF concentration.

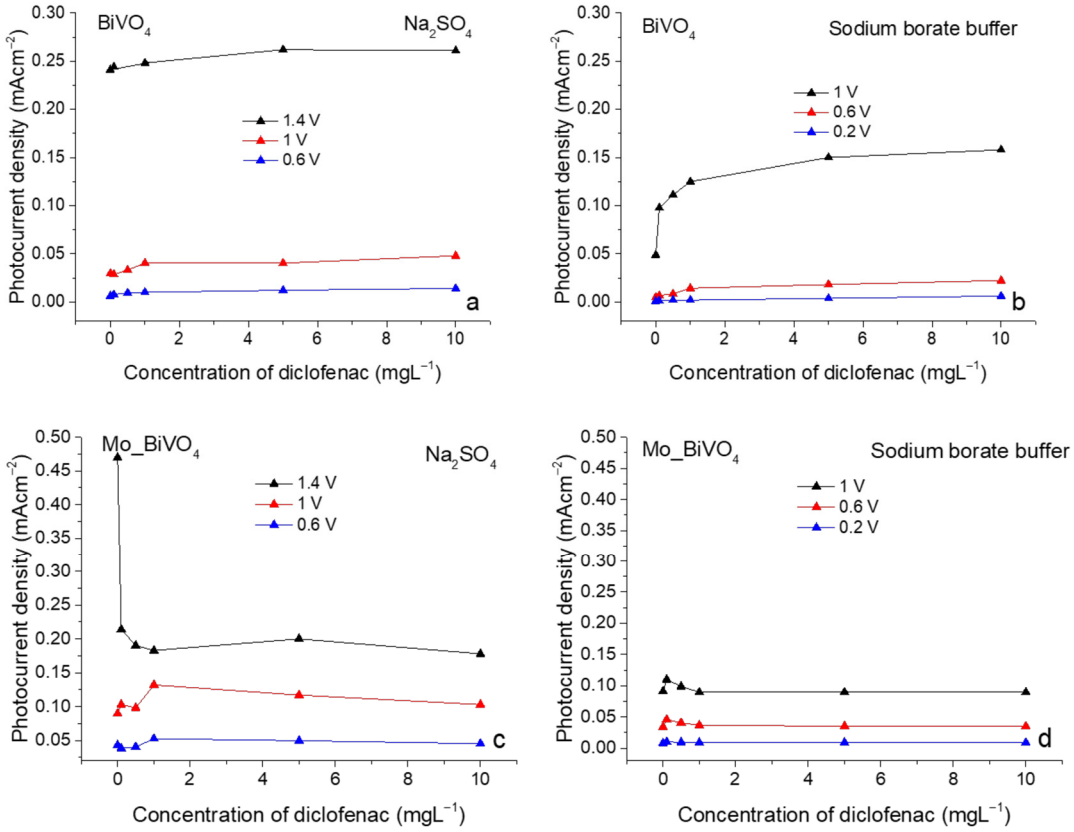

Figure 5. Photocurrent vs. concentration of diclofenac graphs of $BiVO_4$ (**a**,**b**) and Mo_$BiVO_4$ (**c**,**d**) in 0.1 M Na_2SO_4 and 0.2 M sodium borate buffer at different applied potentials.

In order to gain a deeper insight into the distinctive characteristics of the Mo_$BiVO_4$ coating in comparison to the $BiVO_4$ coating, it is essential to perform a comprehensive analysis. Cyclic voltammetry was conducted in electrolytes containing 10 mg L^{-1} of DFC (Figure 6a,b). As can be observed, the red curves corresponding to Mo_$BiVO_4$ coatings exhibit a distinct reduction peak, which was not evident in the initial CVs presented in Figure 3a,b. In the case of the $BiVO_4$ coating, these peaks are also absent. As previously stated, the observed decrease in photocurrent in the Mo_$BiVO_4$ photoanode is likely due to the adsorption of DCF oxidation products on the electrode surface. To ascertain whether DCF and DCF oxidation products were adsorbed on the surface of the photoanode, CVs were recorded in pure sodium sulfate and sodium borate buffer solutions using photoanodes, which underwent chronoamperometric experiments in DCF-containing electrolytes. Prior to CV measurements, the photoelectrodes were rinsed with distilled water and dried. Figure 6c,d demonstrate that the Mo_$BiVO_4$ coatings still exhibit minor reduction peaks, indicating that DCF or oxidation products are still absorbed on the surface of the photoanode, which consequently compromises their sensing performance. Furthermore, the photoresponse of the Mo_$BiVO_4$ coating is reduced by a factor of four in comparison with

the initial CVs (Figure 3a,b). In the case of the pure $BiVO_4$ coating, a small peak is also observed, indicating that DCF remains on the surface of the photoanode as well or that the surface of $BiVO_4$ is altered.

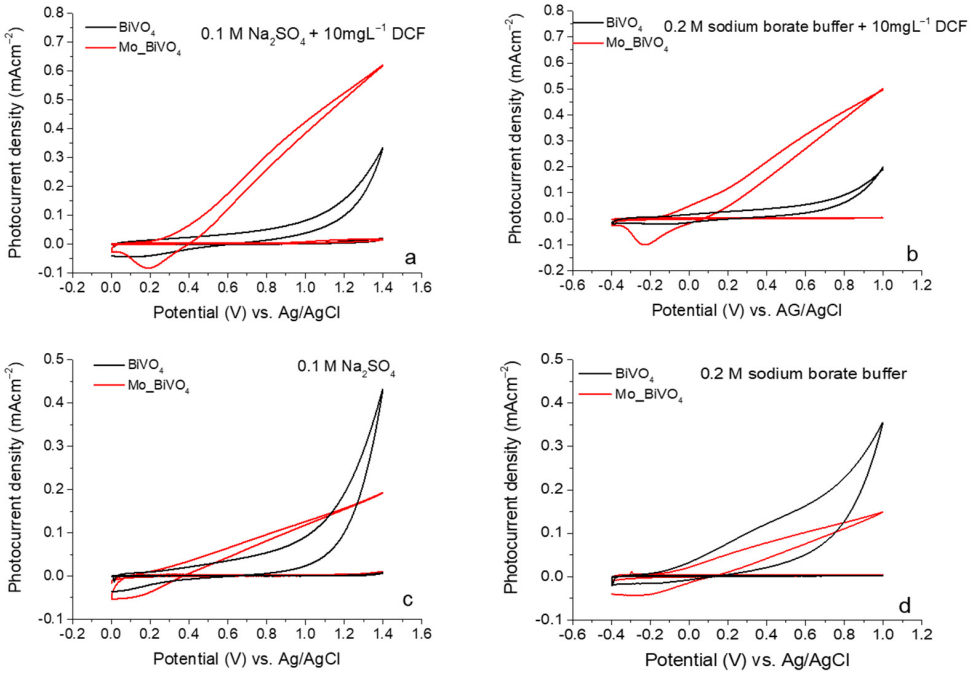

Figure 6. CVs of $BiVO_4$ and Mo_$BiVO_4$ photoanodes in sodium sulfate (**a**) and sodium borate buffer (**b**) containing 10 mg L^{-1} of diclofenac; and in pure sodium sulfate (**c**) and sodium borate buffer (**d**) after PEC sensing performance. Scan rate 50 mV s^{-1}.

A linear relationship between the photocurrent density and the logarithm of DCF concentrations was plotted in Figure 7a,d over the range of 0.1 mg L^{-1} to 10 mg L^{-1} in the SS and SBB electrolytes for $BiVO_4$ and Mo_BiVO4 photoanodes. Correlation coefficients and regression equations are presented in the Table 1. As can be observed, $BiVO_4$ demonstrated a much better linear relationship between photocurrent density and lg of DCF concentration in comparison with the Mo_$BiVO_4$ coating, where regression coefficients were low and reached just 0.25, −0.29, 0.15, and 0.72, 0.85, 0.71 in the SS and SBB electrolytes (Figure 6c,d, Table 1). Higher correlation coefficients were obtained in the SBB, probably due to the absence of sulfate ions—eliminating competing sulfate oxidation reactions—as well as due to changes of pH, which influences several key factors including the band edge positions, reaction kinetics, and surface states, all of which are critical for efficient PEC performance [45,46]. Regression equations I_{ph} = 0.00961 lgC + 0.2512, I_{ph} = 0.00879 lgC + 0.03746, and I_{ph} = 0.00303 lgC + 0.01054 with correlation coefficients 0.83, 0.85, and 0.96, respectively, were obtained in SS, and I_{ph} = 0.03162 lgC + 0.12588, I_{ph} = 0.00787 lgC + 0.01341, and I_{ph} = 0.00236 lgC + 0.00287 with correlation coefficients 0.98, 0.92, and 0.79, respectively, were obtained for $BiVO_4$ in SBB.

The results show that linear correlation was the best for $BiVO_4$ coating in sodium borate buffer at 1 V applied potential and in sodium sulfate electrolyte at 0.6 V, with a limit of detection (LOD) of 6 × 10^{-3} µM and 2.3 × 10^{-3} µM, respectively, based on 3 σ/S, in which σ is the standard deviation of a blank signal and S is the slope of the linear calibration plot presented in Figure 7. In comparison with the previously presented results in Table 2, it can be observed that the use of TiO_2, $CuCo_2O_4$@CoO, and $BiVO_4$/rGO as photoanodes resulted in similar values for the limit of detection of DCF, whereas in the case of heterojunctions TiO_2/$FeVO_4$ and Au/GR-doped CdS lower LODs were found. However, studies investigating the sensing of diclofenac using $BiVO_4$ as a photoanode have not been widely performed.

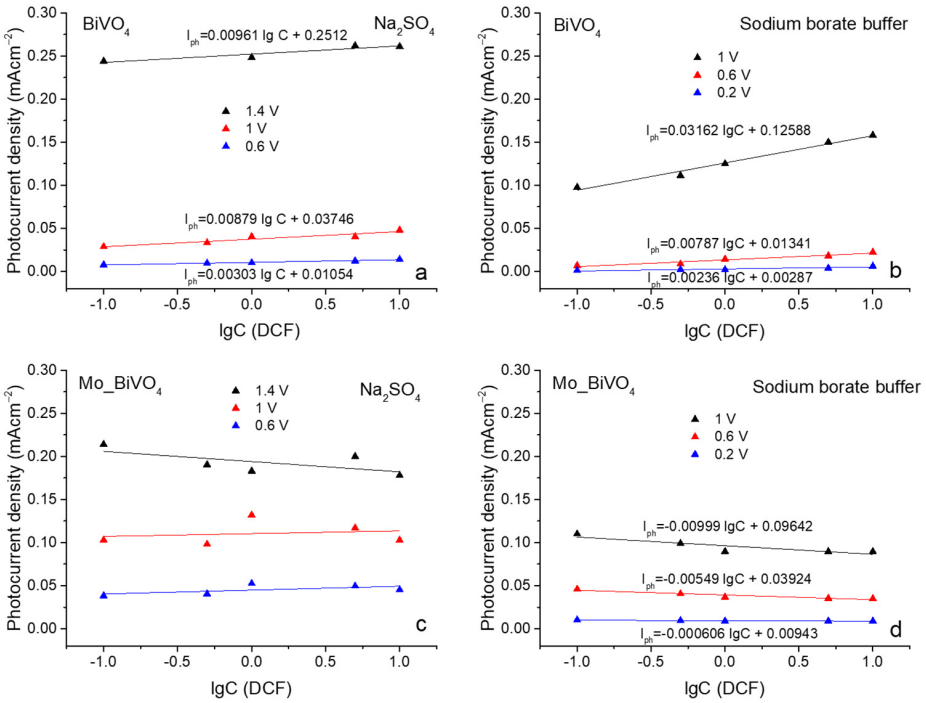

Figure 7. Photocurrent density vs. logarithm of diclofenac concentration in sodium sulfate (**a**,**c**) and sodium borate buffer (**b**,**d**) electrolytes using BiVO4 (**a**,**b**) and Mo_BiVO4 (**c**,**d**) photoanodes.

Table 1. Regression equations and correlation coefficients for $BiVO_4$ and Mo_BiVO_4 coatings at different applied potentials in sodium sulfate and sodium borate buffer.

Photoanode, Electrolyte	Potential, V	Regression Equation	R^2
$BiVO_4$, 0.1 M SS	1.4	I_{ph} = 0.00961 lgC + 0.2512	0.83
	1	I_{ph} = 0.00879 lgC + 0.03746	0.85
	0.6	I_{ph} = 0.00303 lgC + 0.01054	0.96
$BiVO_4$, 0.2 M SBB	1	I_{ph} = 0.03162 lgC + 0.12588	0.98
	0.6	I_{ph} = 0.00787 lgC + 0.01341	0.92
	0.2	I_{ph} = 0.00236 lgC + 0.00287	0.79
Mo_BiVO_4, 0.1 M SS	1.4	I_{ph} = −0.0119 lgC + 0.19401	0.25
	1	I_{ph} = 0.00323 lgC + 0.11036	−0.29
	0.6	I_{ph} = 0.0045 lgC + 0.0449	0.15
Mo_BiVO_4, 0.2 M SBB	1	I_{ph} = −0.00999 lgC + 0.09642	0.72
	0.6	I_{ph} = −0.00549 lgC + 0.03924	0.85
	0.2	I_{ph} = −0.0006062 lgC + 0.00943	0.71

Table 2. Literature overview about photoanodes for detection of diclofenac.

Photoanode	Solution	Detection Range, µM	LOD, µM	Reference
TiO_2	0.1 M Na_2SO_4	5.0×10^{-2}–1.0×10^{3}	3.4×10^{-3}	[47]
$TiO_2/FeVO_4$	0.1 M PBS	1.0×10^{-4}–5.0×10^{-1}	6.9×10^{-5}	[48]
Au/GR doped CdS	0.1 M Na_2SO_4	1.0×10^{-3}–1.5×10^{-1}	7.8×10^{-4}	[21]
$Ni(OH)_2$	1.0 M PBS	2.0×10^{2}–2.7×10^{3}	3.2×10^{1}	[49]
$CuCo_2O_4$@CoO	0.1 M Na_2SO_4	1.0×10^{-2}–5.0×10^{2}	6.5×10^{-4}	[50]
$Cu(OH)_2$	1.0 M PBS	1.8×10^{-1}–1.2×10^{2}	4.0×10^{-2}	[49]
$BiVO_4$/rGO	0.1 M Na_2SO_4	9.6×10^{-3}–9.2×10^{1}	4.2×10^{-3}	[51]

A comparison of the results obtained under different applied bias reveals that the recombination of carriers is more significant at lower applied potentials (see Figures S1 and S2). This is further corroborated by the negative current overshoot observed following the termination of illumination [52]. The results demonstrate that the negative current overshoots observed after the light is switched off are significantly more pronounced in the case of the lower potentials (1 V and 0.6 V in SS and 0.6 V and 0.2 V in SBB) than in the case of the higher potentials. This evidence indicates that the carriers are susceptible to intense surface recombination. This indicates that photogenerated holes do not react with sufficient rapidity with water, sulfate, or organic compounds, thereby increasing the likelihood of recombination with photoelectrons. The rapid decrease in photocurrent observed immediately after illumination and continuing after light cessation is indicative of intense recombination of surface-accumulated holes and electrons. Nevertheless, it is evident that the optimal potential must be selected for the best sensing performance.

3.4. Selectivity Experiments

The $BiVO_4$ photoanode was selected for use in selectivity experiments due to linear correlation of photocurrent versus the logarithm of DCF concentration. Selectivity experiments were conducted in SS and SBB electrolytes, applying 1.4 and 1 V, and 1 and 0.6 V, respectively (Figure 8a,b). In the sodium sulfate electrolyte, an increase in photocurrent was observed when 50 mg L^{-1} of DFC was added. However, after the addition of ibuprofen and dopamine, no discernible changes were noted, indicating that $BiVO_4$ exhibits selectivity for DFC in the sodium sulfate electrolyte. The application of a higher potential resulted in the generation of a greater photocurrent, although the detection of analytes was also observed at lower potentials. In the case of the SBB, a different outcome was observed, with the addition of dopamine resulting in an increase in photocurrent while the addition of ibuprofen did not elicit any changes in the photocurrent. The different selectivity outcomes can be ascribed to the formation of reactive sulfate species (RSS) in the sodium sulfate electrolyte, which exhibits selective reactivity with diclofenac. The results of the experiments demonstrated that the type of electrolyte can exert a significant influence on the selectivity of the sensor.

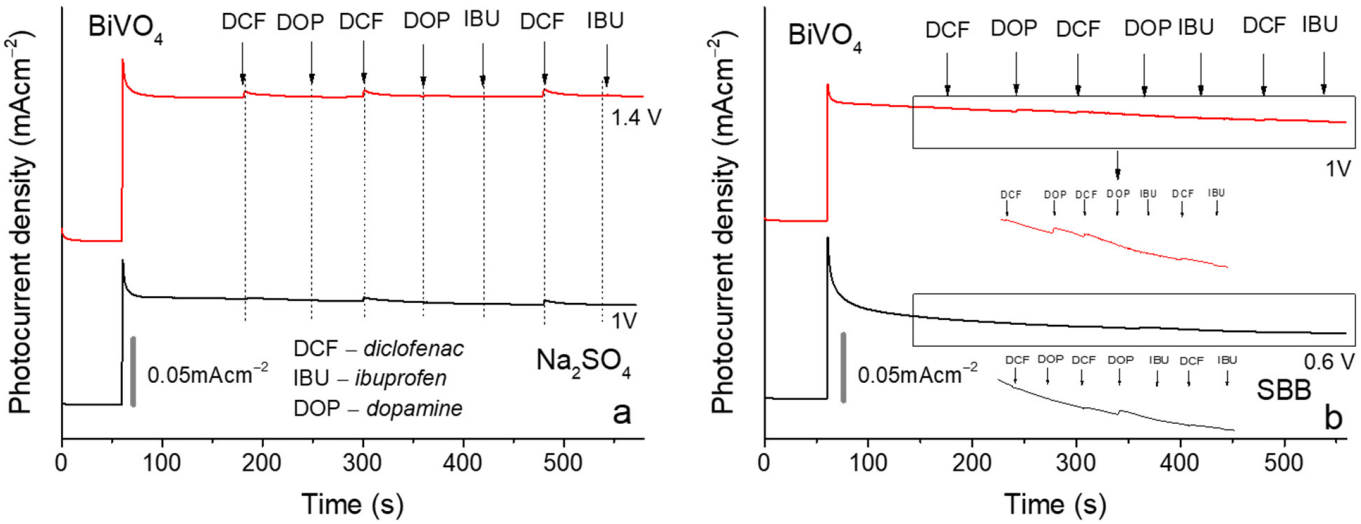

Figure 8. Selectivity experiments were conducted on $BiVO_4$ coatings in Na_2SO_4 (**a**) and sodium borate buffer (**b**). A solution of 50 mg L^{-1} of diclofenac, dopamine, and 5 mg L^{-1} of ibuprofen was added every 60 s. Rectangles mark zoomed sections of curves that are displayed immediately below the rectangle.

4. Conclusions

The objective of this study was to examine the impact of $BiVO_4$ photoanode doping, the nature of the electrolyte, and the applied potential on the sensing performance of DCF. The findings revealed that Mo-doping enhanced the photoelectrochemical activity of the photoanode and reduced the charge transfer resistance. However, the morphological features of the Mo-doped photoanode resulted in the higher adsorption of diclofenac and its oxidation products, which in turn led to the blocking of the surface. Cyclic voltammograms recorded in the sodium sulfate and sodium borate buffer containing 10 mg L^{-1} of DCF and in the pure electrolytes after chopped light illumination experiments demonstrated a reduction peak in the range of 0.4–0 V and −0.4–0 V vs. Ag/AgCl in sodium sulfate and sodium borate buffer, respectively. This confirms adsorption of oxidation products of DCF on the surface of Mo_$BiVO_4$, which are subsequently reduced. A linear correlation was observed between the photocurrent and the logarithm of DCF concentration in the sodium sulfate and sodium borate buffer for the $BiVO_4$ coating at 1 V vs. Ag/AgCl and 0.6 V vs. Ag/AgCl, respectively. In the case of Mo_$BiVO_4$ coatings, a high degree of value distribution was observed. The selectivity experiments demonstrated that $BiVO_4$ is selective for the detection of DCF in a sodium sulfate electrolyte, whereas in a sodium borate buffer, an increase in photocurrent was observed following the addition of dopamine. This discrepancy can be attributed to the nature of the electrolyte. Our study demonstrated that PEC processes can be significantly influenced by such factors as composition and pH of the electrolyte, applied bias, and the surface morphology of the photoactive layer. If the interplay of these factors is properly understood, it may be possible to increase the selectivity of PEC sensors. We hope that our study will be useful for further investigation and modification of $BiVO_4$ in PEC sensing performance.

Supplementary Materials: The following supporting information can be downloaded at: https://www.mdpi.com/article/10.3390/chemosensors12120249/s1, Figure S1: Chronoamperometry under chopped light illumination results in sodium sulfate and sodium borate electrolytes at different applied potentials as photoanode using $BiVO_4$; Figure S2: Chronoamperometry under chopped light illumination results in sodium sulfate and sodium borate electrolytes at different applied potentials as photoanode using Mo_$BiVO_4$.

Author Contributions: Conceptualization, J.J. and A.R.; methodology, M.P.; formal analysis, S.R.; investigation, M.P., I.S. and J.K.-J.; data curation, M.P., I.S., M.S., J.J., S.R. and A.R.; writing—original draft preparation, M.P.; writing—review and editing, J.J. and A.R.; visualization, M.P.; supervision, M.P. and A.R.; funding acquisition, A.R. All authors have read and agreed to the published version of the manuscript.

Funding: This research was funded by the Research Council of Lithuania (LMTLT), agreement No S-PD-22-2.

Institutional Review Board Statement: Not applicable.

Informed Consent Statement: Not applicable.

Data Availability Statement: The data presented in this study are available on request from the corresponding author.

Conflicts of Interest: The authors declare no competing financial interests.

References

1. Lee, D.K.; Choi, K.S. Enhancing Long-Term Photostability of $BiVO_4$ Photoanodes for Solar Water Splitting by Tuning Electrolyte Composition. *Nat. Energy* **2018**, *3*, 53–60. [CrossRef]
2. Khan, A.H.A.; Barros, R. Pharmaceuticals in Water: Risks to Aquatic Life and Remediation Strategies. *Hydrobiology* **2023**, *2*, 395–409. [CrossRef]
3. Samal, K.; Mahapatra, S.; Hibzur Ali, M. Pharmaceutical Wastewater as Emerging Contaminants (EC): Treatment Technologies, Impact on Environment and Human Health. *Energy Nexus* **2022**, *6*, 100076. [CrossRef]

4. Alfonso-Muniozguren, P.; Serna-Galvis, E.A.; Bussemaker, M.; Torres-Palma, R.A.; Lee, J. A Review on Pharmaceuticals Removal from Waters by Single and Combined Biological, Membrane Filtration and Ultrasound Systems. *Ultrason. Sonochem.* **2021**, *76*, 105656. [CrossRef]
5. Nguyen, M.K.; Lin, C.; Nguyen, H.L.; Hung, N.T.Q.; La, D.D.; Nguyen, X.H.; Chang, S.W.; Chung, W.J.; Nguyen, D.D. Occurrence, Fate, and Potential Risk of Pharmaceutical Pollutants in Agriculture: Challenges and Environmentally Friendly Solutions. *Sci. Total Environ.* **2023**, *899*, 165323. [CrossRef]
6. dos Santos, D.F.; Moreira, W.M.; de Araújo, T.P.; Bergamasco, R.; Ostroski, I.C.; de Barros, M.A.S.D. Non-Conventional Processes Applied for the Removal of Pharmaceutics Compounds in Waters: A Review. *Process Saf. Environ. Prot.* **2022**, *167*, 527–542. [CrossRef]
7. Windsor, F.M.; Ormerod, S.J.; Tyler, C.R. Endocrine Disruption in Aquatic Systems: Up-Scaling Research to Address Ecological Consequences. *Biol. Rev.* **2018**, *93*, 626–641. [CrossRef]
8. Deng, H.; Hui, Y.; Zhang, C.; Zhou, Q.; Li, Q.; Du, H.; Hao, D.; Yang, G.; Wang, Q. MXene−derived Quantum Dots Based Photocatalysts: Synthesis, Application, Prospects, and Challenges. *Chinese Chem. Lett.* **2024**, *35*, 109078. [CrossRef]
9. Chander, V.; Sharma, B.; Negi, V.; Aswal, R.S.; Singh, P.; Singh, R.; Dobhal, R. Pharmaceutical Compounds in Drinking Water. *J. Xenobiot.* **2016**, *6*, 5774. [CrossRef]
10. Bruce, G.M.; Pleus, R.C.; Snyder, S.A. Toxicological Relevance of Pharmaceuticals in Drinking Water. *Environ. Sci. Technol.* **2010**, *44*, 5619–5626. [CrossRef]
11. Deng, H.; Wu, Y.; Li, L.; Jiang, X.; Wang, P.; Fang, K.; Li, J.; Hao, D.; Zhu, H.; Wang, Q.; et al. Synergistic Mechanisms for Efficient and Safe Antibiotic Removal: Effective Adsorption and Photocatalytic Degradation Using Aerogels. *Sep. Purif. Technol.* **2025**, *354*, 129455. [CrossRef]
12. Ternes, T.A. Analytical Methods for the Determination of Pharmaceuticals in Aqueous Environmental Samples. *TrAC Trends Anal. Chem.* **2001**, *20*, 419–434. [CrossRef]
13. Neven, L.; Shanmugam, S.T.; Rahemi, V.; Trashin, S.; Sleegers, N.; Carrión, E.N.; Gorun, S.M.; De Wael, K. Optimized Photoelectrochemical Detection of Essential Drugs Bearing Phenolic Groups. *Anal. Chem.* **2019**, *91*, 9962–9969. [CrossRef] [PubMed]
14. Cao, S.; Xie, Z.; Xiao, G.; Sun, X.; Diao, H.; Zhou, X.; Yue, Z. Photoelectrochemical Sensors Based on Heterogeneous Nanostructures for in Vitro Diagnostics. *Biosens. Bioelectron. X* **2022**, *11*, 100200. [CrossRef]
15. Mao, Y.; Liu, X.; Bao, Y.; Niu, L. Recent Advances in Photoelectrochemical Sensors for Analysis of Toxins and Abused Drugs in the Environment. *Chemosensors* **2023**, *11*, 412. [CrossRef]
16. Lv, J.; Chen, X.; Chen, S.; Li, H.; Deng, H. A Visible Light Induced Ultrasensitive Photoelectrochemical Sensor Based on $Cu_3Mo_2O_9$/$BaTiO_3$ P–n Heterojunction for Detecting Oxytetracycline. *J. Electroanal. Chem.* **2019**, *842*, 161–167. [CrossRef]
17. Zarei, M. Sensitive Visible Light-Driven Photoelectrochemical Aptasensor for Detection of Tetracycline Using ZrO_2/g-C_3N_4 Nanocomposite. *Sens. Int.* **2020**, *1*, 100029. [CrossRef]
18. Li, X.; Guo, Z. Development of a Novel Photosensing Method for the Detection of Ciprofloxacin Residues in Athlete's Biological Samples. *Alex. Eng. J.* **2024**, *107*, 675–682. [CrossRef]
19. da Silva Araújo, M.; Barretto, T.R.; Galvão, J.C.R.; Tarley, C.R.T.; Dall'Antônia, L.H.; de Matos, R.; Medeiros, R.A. Visible Light Photoelectrochemical Sensor for Acetaminophen Determination Using a Glassy Carbon Electrode Modified with BiVO4 Nanoparticles. *Electroanalysis* **2021**, *33*, 663–671. [CrossRef]
20. Murugan, E.; Poongan, A. A New Sensitive Electrochemical Sensor Based on $BiVO_4$/ZrO_2@graphene Modified GCE for Concurrent Sensing of Acetaminophen, Phenylephrine Hydrochloride and Cytosine in Medications and Human Serum Samples. *Diam. Relat. Mater.* **2022**, *126*, 109117. [CrossRef]
21. Okoth, O.K.; Yan, K.; Feng, J.; Zhang, J. Label-Free Photoelectrochemical Aptasensing of Diclofenac Based on Gold Nanoparticles and Graphene-Doped CdS. *Sens. Actuators B Chem.* **2018**, *256*, 334–341. [CrossRef]
22. Feng, J.; Li, F.; Qian, Y.; Sun, X.; Fan, D.; Wang, H.; Ma, H.; Wei, Q. Mo-Doped Porous $BiVO_4$/Bi_2S_3 Nanoarray to Enhance Photoelectrochemical Efficiency for Quantitative Detection of 17β-Estradiol. *Sens. Actuators B Chem.* **2020**, *305*, 127443. [CrossRef]
23. Radić, G.; Perović, K.; Sharifi, T.; Kušić, H.; Kovačić, M.; Kraljić Roković, M. Electrochemical Characterisation of the Photoanode Containing TiO_2 and SnS_2 in the Presence of Various Pharmaceuticals. *Catalysts* **2023**, *13*, 909. [CrossRef]
24. Yusuf, T.L.; Ogundare, S.A.; Opoku, F.; Arotiba, O.A.; Mabuba, N. Theoretical and Experimental Insight into the Construction of FTO/$NiSe_2$/$BiVO_4$ Photoanode towards an Efficient Charge Separation for the Degradation of Pharmaceuticals in Water. *J. Environ. Chem. Eng.* **2023**, *11*, 110711. [CrossRef]
25. Li, L.; Li, B.; Liu, H.; Li, M.; Wang, B. Photoelectrochemical Sensing of Hydrogen Peroxide Using TiO_2 Nanotube Arrays Decorated with RGO/CdS. *J. Alloys Compd.* **2020**, *815*, 152241. [CrossRef]
26. Han, F.; Song, Z.; Nawaz, M.H.; Dai, M.; Han, D.; Han, L.; Fan, Y.; Xu, J.; Han, D.; Niu, L. MoS_2/ZnO-Heterostructures-Based Label-Free, Visible-Light-Excited Photoelectrochemical Sensor for Sensitive and Selective Determination of Synthetic Antioxidant Propyl Gallate. *Anal. Chem.* **2019**, *91*, 10657–10662. [CrossRef]
27. Vinothkumar, V.; Sangili, A.; Chen, S.M.; Abinaya, M. Additive-Free Synthesis of $BiVO_4$ Microspheres as an Electrochemical Sensor for Determination of Antituberculosis Drug Rifampicin. *Colloids Surfaces A Physicochem. Eng. Asp.* **2021**, *624*, 126849. [CrossRef]

28. Petruleviciene, M.; Savickaja, I.; Juodkazyte, J.; Ramanavicius, A. Investigation of WO_3 and $BiVO_4$ Photoanodes for Photoelectrochemical Sensing of Xylene, Toluene and Methanol. *Chemosensors* **2023**, *11*, 552. [CrossRef]
29. Okoth, O.K.; Yan, K.; Zhang, J. Mo-Doped $BiVO_4$ and Graphene Nanocomposites with Enhanced Photoelectrochemical Performance for Aptasensing of Streptomycin. *Carbon* **2017**, *120*, 194–202. [CrossRef]
30. Singh, P.; Sharma, S.; Devi, P. 2D Nanomaterial Photoelectrodes for Photoelectrochemical Degradation of Pollutants and Hydrogen Generation. In *Two-Dimensional Materials for Environmental Applications*; Springer: Cham, Switzerland, 2023; Volume 332, pp. 299–325.
31. Vicenteno-Vera, A.G.; Campos-Hernandez, T.; Ramirez-Silva, M.T.; Galano, A.; Rojas-Hernandez, A. Determination of pKa Values of Diclofenac and Ibuprofen in Aqueous Solutions by Capillary Zone Electrophoresis. *ECS Trans.* **2010**, *29*, 443–448. [CrossRef]
32. Chang, E.D.; Town, R.M.; Owen, S.F.; Hogstrand, C.; Bury, N.R. Effect of Water pH on the Uptake of Acidic (Ibuprofen) and Basic (Propranolol) Drugs in a Fish Gill Cell Culture Model. *Environ. Sci. Technol.* **2021**, *55*, 6848–6856. [CrossRef] [PubMed]
33. Balu, S.; Chen, Y.L.; Chen, S.W.; Yang, T.C.K. Rational Synthesis of $Bi_xFe_1-xVO_4$ Heterostructures Impregnated Sulfur-Doped G-C_3N_4: A Visible-Light-Driven Type-II Heterojunction Photo(electro)catalyst for Efficient Photodegradation of Roxarsone and Photoelectrochemical OER Reactions. *Appl. Catal. B Environ.* **2022**, *304*, 120852. [CrossRef]
34. Monfort, O.; Plesch, G. Bismuth Vanadate-Based Semiconductor Photocatalysts: A Short Critical Review on the Efficiency and the Mechanism of Photodegradation of Organic Pollutants. *Environ. Sci. Pollut. Res.* **2018**, *25*, 19362–19379. [CrossRef] [PubMed]
35. Pradhan, D.; Biswal, S.K.; Singhal, R.; Panda, P.k.; Dash, S.K. Green Nanoarchitectonics Ce-Co_3O_4/$BiVO_4$ (P-N) Heterojunction Nanocomposite: Dual Functionality for Photodegradation of Congo Red and Supercapacitor Applications. *Surf. Interfaces* **2024**, *52*, 104954. [CrossRef]
36. Wang, L.; Li, Z.; Wang, K.; Dai, Q.; Lei, C.; Yang, B.; Zhang, Q.; Lei, L.; Leung, M.K.H.; Hou, Y. Tuning D-Band Center of Tungsten Carbide via Mo Doping for Efficient Hydrogen Evolution and Zn–H_2O Cell over a Wide pH Range. *Nano Energy* **2020**, *74*, 104850. [CrossRef]
37. Xu, H.; Fan, W.; Zhao, Y.; Chen, B.; Gao, Y.; Chen, X.; Xu, D.; Shi, W. Amorphous Iron (III)-Borate Decorated Electrochemically Treated-BiVO4 Photoanode for Efficient Photoelectrochemical Water Splitting. *Chem. Eng. J.* **2021**, *411*, 128480. [CrossRef]
38. Ruan, G.; Ghosh, P.; Fridman, N.; Maayan, G. A Di-Copper-Peptoid in a Noninnocent Borate Buffer as a Fast Electrocatalyst for Homogeneous Water Oxidation with Low Overpotential. *J. Am. Chem. Soc.* **2021**, *143*, 10614–10623. [CrossRef]
39. Petruleviciene, M.; Savickaja, I.; Juodkazyte, J.; Grinciene, G.; Ramanavicius, A. Investigation of $BiVO_4$-Based Advanced Oxidation System for Decomposition of Organic Compounds and Production of Reactive Sulfate Species. *Sci. Total Environ.* **2023**, *875*, 162574. [CrossRef]
40. Petruleviciene, M.; Parvin, M.; Savickaja, I.; Gece, G.; Naujokaitis, A.; Pakstas, V.; Pilipavicius, J.; Gegeckas, A.; Gaigalas, G.; Juodkazyte, J. WO_3 Coatings for Photoelectrochemical Synthesis of Persulfate: Efficiency, Stability and Applicability. *J. Solid State Electrochem.* **2022**, *26*, 1021–1035. [CrossRef]
41. Petruleviciene, M.; Turuta, K.; Savickaja, I.; Juodkazyte, J.; Ramanavicius, A. Photoelectrochemical Degradation of Organic Compounds via Formed Reactive Chlorine and Sulfate Species by WO_3-Based Photoanodes. *J. Electroanal. Chem.* **2023**, *951*, 117954. [CrossRef]
42. Parvin, M.; Petrulevičienė, M.; Savickaja, I.; Šebeka, B.; Karpicz, R.; Grigucevičienė, A.; Ramanauskas, R.; Juodkazytė, J. Influence of Morphology on Photoanodic Behaviour of WO_3 Films in Chloride and Sulphate Electrolytes. *Electrochim. Acta* **2022**, *403*, 139710. [CrossRef]
43. Zhang, S.; Ahmet, I.; Kim, S.H.; Kasian, O.; Mingers, A.M.; Schnell, P.; Kölbach, M.; Lim, J.; Fischer, A.; Mayrhofer, K.J.J.; et al. Different Photostability of $BiVO_4$ in near-pH-Neutral Electrolytes. *ACS Appl. Energy Mater.* **2020**, *3*, 9523–9527. [CrossRef] [PubMed]
44. Fan, Z.; Fan, L.; Shuang, S.; Dong, C. Highly Sensitive Photoelectrochemical Sensing of Bisphenol a Based on Zinc phthalocyanine/TiO_2 Nanorod Arrays. *Talanta* **2018**, *189*, 16–23. [CrossRef] [PubMed]
45. Tayyebi, A.; Soltani, T.; Lee, B.K. Effect of pH on Photocatalytic and Photoelectrochemical (PEC) Properties of Monoclinic Bismuth Vanadate. *J. Colloid Interface Sci.* **2019**, *534*, 37–46. [CrossRef]
46. Das, P.K.; Arunachalam, M.; Seo, Y.J.; Ahn, K.S.; Ha, J.S.; Kang, S.H. Electrolyte Effects on Undoped and Mo-Doped $BiVO_4$ Film for Photoelectrochemical Water Splitting. *J. Electroanal. Chem.* **2019**, *842*, 41–49. [CrossRef]
47. Bai, X.; Gao, W.; Zhou, C.; Zhao, D.; Zhang, Y.; Jia, N. Photoelectrochemical Determination of Diclofenac Using Oriented Single-Crystalline TiO_2 Nanoarray Modified with Molecularly Imprinted Polypyrrole. *Microchim. Acta* **2022**, *189*, 90. [CrossRef]
48. Yang, L.; Li, L.; Li, F.; Zheng, H.; Li, T.; Liu, X.; Zhu, J.; Zhou, Y.; Alwarappan, S. Ultrasensitive Photoelectrochemical Aptasensor for Diclofenac Sodium Based on Surface-Modified TiO_2-$FeVO_4$ Composite. *Anal. Bioanal. Chem.* **2021**, *413*, 193–203. [CrossRef]
49. Arvand, M.; Gholizadeh, T.M.; Zanjanchi, M.A. MWCNTs/$Cu(OH)_2$ nanoparticles/IL Nanocomposite Modified Glassy Carbon Electrode as a Voltammetric Sensor for Determination of the Non-Steroidal Anti-Inflammatory Drug Diclofenac. *Mater. Sci. Eng. C* **2012**, *32*, 1682–1689. [CrossRef]
50. Wang, Q.; Jiang, M.; Zhang, L. Label-Free and Visible-Light Driven Photoelectrochemical Sensor with $CuCo_2O_4$@CoO Core-Shell Hybrid Rod as Photoanode for Selective Sensing Diclofenac. *Electrochim. Acta* **2021**, *397*, 139239. [CrossRef]

51. do Prado, T.M.; Cincotto, F.H.; Fatibello-Filho, O.; Cruz de Moraes, F. Bismuth Vanadate/Reduced Graphene Oxide Nanocomposite Electrode for Photoelectrochemical Determination of Diclofenac in Urine. *Electroanalysis* **2018**, *30*, 2704–2711. [CrossRef]
52. Feng, F.; Mitoraj, D.; Gong, R.; Gao, D.; Elnagar, M.M.; Liu, R.; Beranek, R.; Streb, C. High-Performance $BiVO_4$ Photoanodes: Elucidating the Combined Effects of Mo-Doping and Modification with Cobalt Polyoxometalate. *Mater. Adv.* **2024**, *5*, 4932–4944. [CrossRef]